



HAL
open science

**Effects of various surface treatments on Aloe Vera fibers
used as reinforcement in
poly(3-hydroxybutyrate-co-3-hydroxyhexanoate)
(PHBHHx) biocomposites**

Nadjet Dehouche, Celia Idres, Mustapha Kaci, Idris Zembouai, Stéphane
Bruzaud

► **To cite this version:**

Nadjet Dehouche, Celia Idres, Mustapha Kaci, Idris Zembouai, Stéphane Bruzaud. Effects of various surface treatments on Aloe Vera fibers used as reinforcement in poly(3-hydroxybutyrate-co-3-hydroxyhexanoate) (PHBHHx) biocomposites. *Polymer Degradation and Stability*, 2020, 175, pp.109131 -. 10.1016/j.polymdegradstab.2020.109131 . hal-03489636

HAL Id: hal-03489636

<https://hal.science/hal-03489636>

Submitted on 20 May 2022

HAL is a multi-disciplinary open access archive for the deposit and dissemination of scientific research documents, whether they are published or not. The documents may come from teaching and research institutions in France or abroad, or from public or private research centers.

L'archive ouverte pluridisciplinaire **HAL**, est destinée au dépôt et à la diffusion de documents scientifiques de niveau recherche, publiés ou non, émanant des établissements d'enseignement et de recherche français ou étrangers, des laboratoires publics ou privés.



Distributed under a Creative Commons Attribution - NonCommercial 4.0 International License

Effects of Various Surface Treatments on Aloe Vera Fibers Used as Reinforcement in Poly(3-Hydroxybutyrate-Co-3-Hydroxyhexanoate) (PHBHHx) Biocomposites

Nadjet Dehouche¹, Celia Idres¹, Mustapha Kaci¹, Idris Zembouai¹, Stéphane Bruzaud^{2*}

¹Laboratoire des Matériaux Polymères Avancés (LMPA), Université de Bejaia, 06000, Algeria

²Institut de Recherche Dupuy de Lôme (IRDL), UMR CNRS 6027, Université de Bretagne-Sud, Rue Saint Maudé, 56321 Lorient Cedex, France

* Corresponding author: stephane.bruzaud@univ-ubs.fr

Abstract

The aim of this study was to assess the effect of various surface treatments on Aloe Vera fibers (AVF) used as reinforcement in PHBHHx biocomposites prepared by melt compounding. AVF were subjected to various surface treatments including alkaline, organo-silanes and combined alkaline/organo-silanes treatments. Both untreated and treated AVF were added to PHBHHx at filler content of 20 wt.% and the resulted biocomposites were characterized using scanning electron microscopy (SEM), differential scanning calorimetry (DSC), thermogravimetric analysis (TGA), water absorption test and rheological measurements. The study showed that the combined alkaline/organo-silanes treatment of AVF resulted in better morphology and properties of PHBHHx biocomposite compared to untreated AVF and those treated either with alkaline or with organosilanes. Indeed, SEM analysis of the fracture surface of PHBHHx/AVF treated with combined alkaline-organosilanes showed better fiber-matrix interactions compared to the other samples. As a result, rheological properties, i.e., complex viscosity (η^*), storage modulus (G') and loss modulus (G'') were increased. Higher resistance to water absorption was observed for PHBHHx/AVF treated with combined alkaline-organosilanes. Whereas, the various surface

fiber treatments led to no noticeable change in thermal characteristics of the biocomposites. This study highlights the effectiveness of combined alkaline/organo-silanes treatment of AVF over alkaline and organo-silanes and their applications in PHBHHx biocomposites as an interesting source of cellulosic reinforcing materials.

Keywords: PHBHHx, Aloe Vera fibers (AVF), Biocomposites, Fiber surface treatment, Morphology.

1. Introduction

In recent years, biodegradable polymers and natural fibers are gaining growing interest from both industry and academia towards developing environmentally friendly materials as an alternative to petroleum based products [1]. In addition, natural fiber reinforced polymer composite technology focuses also on low cost and performance [2]. Hence, the use of original raw materials should be defined in terms of sustainability to elaborate new products based on biocomposites [3]. New developments in the field of renewable and biodegradable polymers are being intensified. In this context, polyhydroxyalcanoates (PHA) are derived from renewable resources and are fully biodegradable thermoplastics [4]. They are totally synthesized by microorganism as an intracellular storage product [5,6]. Under, specific conditions of nitrogen limitation and an excess of carbon food source, which can be a saccharide (sugar), the bacteria transform the excess of their feeding into intracellular grains of polymer and stored in the cell cytoplasm [5–8]. The main limitations of PHA to extend their industrial applications are mainly high thermal sensitivity and low mechanical resistance [9]. To overcome these drawbacks, block copolymers have been developed introducing different monomeric units in PHAs. This is the case of poly(3-hydroxybutyrate-co-3-hydroxyhexanoate) (PHBHHx), which is a random copolymer of 3-hydroxybutyrate and 3-

hydroxyhexanoate [7]. Due to its ductile nature and wider processing window compared to poly(3-hydroxybutyrate), PHBHHx has a broad range of applications in various industries such as biomedical sector including tissue engineering, bio-implant patches, drug delivery, surgery, wound dressing and scaffolds, agriculture in the controlled release of insecticides and also flexible packaging [7,10]. Together with the developments of new biopolymers, an increasing interest on natural fiber reinforced bioplastics has been observed [11]. Among the biodegradable reinforcements, a new kind of natural cellulosic fibers is extracted from the leaves of Aloe Vera Cactus plant, which is a member of the Agavoideae family [12]. This plant is largely available in the North African countries, especially in Algeria and it represents an interesting source of cellulosic reinforcing materials [13]. Aloe Vera plant is widely cultivated throughout the world for its gel. It is also used in cosmetic and pharmaceutical industry and more recently in textile industry in India [14]. Although, there have been some studies on the characterization and chemical treatment of Aloe Vera Cactus fibers [12,13], their use as a cellulosic reinforcing material in polymeric materials, particularly in biodegradable polymers, is rather scarce. Only a few papers reported the use of Aloe Vera fibers as a reinforcement in PLA matrix [15]. Accordingly, the authors indicated that the properties of Aloe Vera and sisal fibers reinforced biocomposites are comparable. Further, both types of fibers significantly improved the mechanical behavior of PLA. However, there is a major limitation of using cellulosic fibers in polymer composites applications due to high moisture absorption or release and poor dimensional stability of the natural fibers [16,17]. In addition, due to the hydrophilic character of the cellulosic fibers by the presence of hydroxyl and other polar groups, it remains difficult to ensure a homogeneous dispersion of these natural fillers in a hydrophobic polymer matrix during melt compounding process. The effectiveness of natural fibers as reinforcement can be improved by enhancing the interfacial adhesion between the fiber and the polymer matrix through various fiber surface treatments

including alkaline treatment, silane treatment, acetylation treatment, benzylation treatment and peroxide treatment [18]. Among these, the silanization is one of the most commonly used surface treatments for natural fiber surface modification, especially for the nanocellulose fibers due to the ability of silanes to interact with both natural fibers and composite matrix [19]. This study investigates the effects of Aloe Vera fiber surface treatment, including alkaline treatment, organo-silanes treatment and a combined alkaline-organosilanes treatment, on the morphology and thermal and rheological properties of PHBHHx/Aloe Vera fiber biocomposites incorporated at 20 wt.%. The nominal composition of 20 wt. % of AVF was used as an intermediate one. Moreover beyond 30 wt. % of cellulosic fibers, it becomes difficult to feed the fibers and process the biocomposites with conventional techniques such as extrusion and injection molding machines [15].

2. Experimental part

2.1. Materials used

PHBHHx containing 11 wt.% of hydroxyhexanoate was provided in pellets by Kaneka Corporation (Westerlo-Oevel, Belgium) under the trade name Aonilex X151A. According to the manufacturer, this grade is white in color. The main physical characteristics of the polymer are as follows: density = 1.19 g/cm³, melting temperature (T_m) = 130°C, glass transition temperature (T_g) = -0.2°C and crystallinity index (X_c) = 34%. The chemical structure of PHBHHx is given in scheme 1.

Scheme 1

Fibers were extracted from Aloe Vera leaves (AVL), which have been collected in the region of Bejaia in Algeria. The detailed extraction procedure of the fibers is given in section 2.2.

Trimethoxy-octadecyl-silanes (TMOS) purchased from Sigma-Aldrich (France) was used to modify the surface of AVF for better adhesion with hydrophobic polymer matrix [20]. The chemical structure of TMOS is $\text{CH}_3(\text{CH}_2)_{17}\text{Si}(\text{OCH}_3)_3$ and the molar mass is $374.67 \text{ g mol}^{-1}$.

2.2. Aloe Vera fibers (AVF) extraction procedure

The fibers were extracted from the leaves of Aloe Vera cactus illustrated in Figure 1.

Figure 1

The AVF extraction procedure was carried out using water retting according to the procedure described by Mannai et al. [21] and shown in Figure 2. The procedure was as follows:

Figure 2

Before immersing AVL in water bath, the remaining pith and cortex parenchyma of the plant were completely removed. In order to separate the Aloe Vera fibers from the stems, the leaves were first cut into small pieces and washed as shown in step (a) in Figure 2. The Aloe Vera pieces were then immersed in a thermostatically controlled water bath at 90°C for 2h to inhibit the enzymes effect. In the next step (b), the recovered pieces were placed in a closed water container for 15–20 days. In the last step (c), the fibers were then easily extracted from the leaf pieces and washed with distilled water to remove the pulp and contaminants on the surface before drying them in an oven at 70°C overnight.

2.3. Chemical composition of Aloe Vera fibers (AVF)

The chemical composition of AVF was determined according to the experimental procedure reported in literature [22,23]. The main chemical composition of AVF are the following: cellulose = 64.9 wt.%, lignin = 4.1 wt.%, hemicelluloses = 25.1 wt.% and extractives = 5.9 wt.%. Moreover, the measured density of AVF = 1.4325, which is very close to that reported by Balaji et al. [12].

2.4. AVF surface treatments

2.4.1. Alkaline treatment with NaOH

Alkaline treatment of AVF was carried out in order to eliminate the hemicellulose, the pectin and partially or totally the lignin, according to the procedure described in literature [12,24]. Prior to any surface treatment, AVF were dried in a vacuum oven at 70°C overnight. The initial fibers were cut to a few millimeters length (~1-2 mm). The short fibers were subjected to a surface treatment in a NaOH solution at 5 wt. %. The temperature was kept constant at 27°C during 1h under atmospheric pressure and a moderate agitation. The fibers were removed from the alkaline solution, filtered and washed with distilled water for several times. After this, the fibers were rinsed by a 2 wt. % acetic acid solution until getting a neutral pH. The washed fibers were then dried at 70°C until getting a constant mass.

2.4.2. Organosilanes treatment by TMOS

The treatment consisted of grafting TMOS molecules onto the AVF surface according to the procedure described in literature [25,26]. 4g of AVF were sonicated in a 100 ml solution of water/ethanol (70/30 v/v) mixture for 1h. Along with this, 2 wt.% of TMOS based on the mass of AVF used, were also dissolved in a separate 100 ml of water/ethanol (70/30 v/v) solution for 1h, while adjusting the pH to 4 with glacial acetic acid. The sonicated AVF were soaked in TMOS solution at room temperature and a continuous stirring for 3 h. Finally, AVF were removed from the solution, filtered and dried in an oven at 110°C for 12 h for a complete condensation of silanol groups [23].

2.4.3. Combined NaOH-organosilanes treatment

In this treatment, the procedure consisted of subjecting alkaline treated AVF to organosilanes treatment by TMOS using the same experimental procedure previously described.

2.5. Preparation of PHBHHx/AVF biocomposites by melt compounding

In order to minimize both the moisture effect and hydrolysis on PHBHHx and AVF, all materials were dried in a vacuum oven at 70°C for 12 h before processing. The preparation of PHBHHx/AVF biocomposites before and after fiber surface treatment was carried out in a

twin-screw micro-compounder, Model DSM Xplore (version 1.0 - 2005) at 145°C and 50 rpm. AVF were incorporated into PHBHHx at loading rate of 20 wt.%. The code and composition of the neat PHBHHx and the biocomposite samples elaborated with various fiber surface treatments are given in Table 1.

Table 1

2.6. Characterization Techniques

2.6.1. Scanning electron microscopy (SEM)

Fracture surface morphology of the biocomposite samples and the AVF surface before and after treatments were observed by using a Jeol JSM-6031 scanning electron microscope. The neck region for the broken biocomposite samples fractured in liquid nitrogen is parallel to the draw direction in order to reveal the internal morphology. Prior to any observation, the fracture surfaces were coated with a thin gold layer by means of a Polaron sputtering apparatus.

2.6.2. Attenuated total reflectance-infrared spectroscopy (ATR-IR)

ATR-IR spectra of AVF before and after alkaline treatment were recorded using an Agilent technology Cary 630 FTIR spectrometer at 8 cm⁻¹ resolution and 64 scans. All spectra were recorded in the absorbance mode in the 4000 - 600 cm⁻¹ region.

2.6.3. Thermogravimetric analysis (TGA)

TGA experiments were carried out in a thermal analyzer (Setaram TGDTA92-10) using a heating rate of 10°C/min under nitrogen atmosphere in the temperature range starting from 20 to 600°C for the PHBHHx/AVF biocomposite samples, while the temperature started from 20 to 800°C for AVF. The TGA data represent the average of three replicates.

2.6.4. Differential Scanning Calorimetry (DSC)

DSC analyzes were performed on weighted samples of about 15 mg using a differential scanning calorimeter (Mettler-Toledo DSC-882 Model). The samples were first heated from -

40 to +200°C at a heating rate of 20°C/min in inert atmosphere (N₂) and kept at this temperature for 2 min to eliminate thermal history. The samples were then cooled to -40°C at a cooling rate of 20°C/min. Then the samples were heated again to +200°C at 20°C/min so that the melting could be studied. Indeed, the second thermal cycle provides accurate results on the glass transition temperature (T_g), the melting temperature (T_m) measured from the peak value of the endotherm, the cold crystallization temperature (T_{cc}), measured from the lowest peak value of the exotherm, melting enthalpy (ΔH_m) and enthalpy of cold crystallization (ΔH_{cc}). The DSC values represent the average of three replicates.

2.6.5. Rheological measurements

Rheological measurements were performed using an Anton Paar MCR301 rheometer. Sample disks were vacuum-dried at 60°C for 24h prior to testing. Rheological experiments were performed at 150°C using a 25 mm parallel plate system. The disks were equilibrated for 4 min before the gap was set to the testing position of 0.95mm. The limit of the linear viscoelastic regime was determined by performing a strain sweep at 1 Hz. A strain of 0.5%, corresponding to the linear viscoelastic domain, was chosen to perform dynamic measurements over a frequency range from 0.01 to 100 Hz.

2.6.6. Water absorption test

The water absorption percentage was determined by measuring the difference between the weight at the initial time of the test and the constant final weight of the sample at a given time according to ASTM D570-98 (2018) standard method. The sample dimensions were 10x10x1.0 mm. The samples were dried in a vacuum oven at 70°C overnight, cooled in a desiccator, and immediately weighed using a four digit balance. The conditioned samples were then immersed in distilled water at room temperature. The samples were removed regularly, blotted to eliminate excess water on the surface and weighted. The percentage of water absorption (WA %) was calculated according to eq.(1) [27].

$$W_A(\%) = \frac{m_t - m_0}{m_0} \times 100\% \quad (1)$$

Where W_A is the water absorption in %, m_t is the sample weight after a given immersion time, and m_0 is the initial weight sample before immersion. The average scatter around the mean value was $\pm 0.1\%$.

3. Results and discussion

3.1. Aloe Vera fibers (AVF) characterization

To make effective use of AVF as reinforcement in composite materials, the fiber surface modification must be performed to obtain an enhanced interface between the hydrophilic AVF and PHBHHx. Thus, chemical structure, morphology and thermal stability of AVF were characterized before and after surface treatment by FTIR spectroscopy, SEM and TGA, respectively.

3.1.1. ATR-IR analysis of AVF

ATR-IR spectroscopy was used to track changes in the chemical structure of the fibers. In this respect, Figure 3 shows comparative ATR-IR spectra of untreated AVF and those treated with alkaline, organo-silanes and combined alkaline/organo-silanes.

Figure 3

From Figure 3, the ATR-IR spectra of untreated AVF exhibit the presence of a large absorption band at 3300 cm^{-1} which is attributed to the free hydroxyl groups ($-\text{OH}$) [28]. Furthermore, there is also the presence of an absorption band at 2900 cm^{-1} assigned to $-\text{CH}$ stretching of methyl and methylene groups [15]. The characteristic absorption bands centered at 1728 cm^{-1} and 1246 cm^{-1} correspond to the $\text{C}=\text{O}$ stretching vibration and $\text{C}-\text{O}$ stretching bond of hemicellulose, pectin and lignin contained in AVF [28]. After surface treatment of the fibers, it is observed in Figure 3, a decrease in the absorption band intensity at 3300 cm^{-1} for both the alkaline and organosilanes indicating that the number of hydroxyl groups on the

fiber surface has decreased. Moreover, it is observed in the alkaline treated AVF fibers, the disappearance of the absorption bands centered at 1728 and 1246 cm^{-1} , which indicates that the hemicellulose and a part of lignin components in the AVF are eliminated [24]. For the combination of alkaline-organosilanes treated AVF, the absorption band intensity at 3300 cm^{-1} becomes stronger due to the presence of silanol groups [29]. From the medallion in Fig. 3, a small shoulder located at roughly 769 cm^{-1} is noticed on both ATR-IR spectra of silane and combined alkaline-silane treated fibers, which is assigned to Si-O-Si groups resulting from self-condensation of a very small amount of TMOS on AVF surface [30,31]. The ATR-IR data show clearly the effect of each type of surface treatment on the structure of AVF with respect to alkaline, organo-silanes and combined alkaline-organosilanes treatments [12].

3.1.2. Surface morphology of AVF

Figure 4(a) and (b) shows the SEM micrographs of surface morphology of AVF before and after alkaline treatment, respectively. (The SEM micrographs of organo-silanes and combined alkaline/organosilanes treated fibers are not shown because similar surface morphology of the fibers is observed as the alkaline treated fibers).

Figure 4(a) and (b)

It is observed in Figure 4(a) that the untreated AVF shows a homogeneous and compact surface with fewer irregularities compared with the alkaline treated one displayed in Figure 4(b). Indeed, the presence of pectin, lignin, and other extractible on the fiber surface provides certain smoothness. After alkaline treatment, the fiber surface becomes rough and it is characterized by the formation of wide and deep grooves, while the fiber diameter is variable as shown in Figure 4(b). This may result from the fibrillation of AVF, delignification and elimination of impurities [32]. As reported in literature [21], alkaline treatment leads to breaking down the fiber bundle into smaller fibres with a rough surface topography. As a

result, the fiber/matrix interface is enhanced and subsequently, mechanical properties are improved.

3.1.3. Thermal stability

Thermal stability of untreated and treated AVF was investigated by TGA under N₂ atmosphere. Figure 5 shows DTG thermograms of untreated and treated AVF.

Figure 5

From Figure 5, it is observed that DTG curves display a broad peak in the temperature range 50-100°C for all treated and untreated fibers. This is attributed to the loss of a small amount of weight due to the evaporation of moisture present in the fibers. Furthermore, the untreated fibers exhibit a lower temperature peak at around 295°C which is related to the decomposition of hemicellulose. For the alkaline treated fibers, this peak disappears totally indicating that the hemicellulose is fully removed from the fibers [22]. For the combined alkaline and organo-silanes treated fibers, the peak is not visible at 295°C, but another peak appears at lower temperature at approximately 215°C, which is due to the removal of the moisture generated from the self-condensation reactions of the residual Si-OH groups and also to the partial removal of uncrosslinked oligomers (Si-O-Si) [30]. On the other hand, the DTG curves of organo-silanes treated fibers exhibit both temperature peaks, i.e., 215 and 295°C. Furthermore, a strong temperature peak is observed at 350°C for the untreated AVF. The peak intensity increases significantly after the alkaline treatment of the fibers. For the organosilanes and combined alkaline-organosilanes treated fibers; besides a large increase in the peak intensity, its position shifts towards lower temperature by almost 17°C compared to that of untreated fibers. According to Chowdhury et al. [33], the peaks observed in the temperature range 333-350°C correspond to those of cellulose, whereas lignin decomposes slowly at higher temperature. The presence of lignin is the cause of production of the char, which is the product at the end of the pyrolysis process [25].

3.2. Characterization of PHBHHx/AVF biocomposites

3.2.1. Morphological analysis

The fracture surface of PHBHHx filled with untreated and treated AVF were examined by SEM. In this regard, Figure 6(a), (b), (c), (d) and (e) shows the SEM micrographs of the fracture surfaces of neat PHBHHx, PHBHHx/untreated AVF, PHBHHx/alkaline-treated AVF, PHBHHx/organosilanes-treated AVF, and PHBHHx/combined alkaline-organosilanes treated AVF biocomposites, respectively.

Figure 6(a), (b), (c), (d) and (e)

In Figure 6(a), the fracture surface of PHBHHx is homogeneous and compact, although some defects are visible, which are due probably to the fracturing procedure. For PHBHHx/untreated AVF biocomposite shown in Figure 6(b), it is clearly observed the formation of aggregates randomly distributed in the polymer matrix. Furthermore, AVF are pulled out from the PHBHHx surface indicating a low interfacial adhesion between the fibers and the matrix [26]. Other defects such as craters and microvoids are also present on the fracture surface of the biocomposite, which indicate the non compatibility of PHBHHx and AVF [16].

Figure 6(c) shows the fracture surface of PHBHHx/AVF treated with alkaline. Microscopic holes and cavities are observed on the fracture surface of PHBHHx along with alkaline-treated AVF are dispersed randomly in the matrix. This could be related to an insufficient adhesion of the fibers to the polymer matrix. In Figure 6(d) relative to the PHBHHx/organosilanes treated AVF, a noticeable change in the surface morphology of the biocomposite is clearly observed compared to Figure 6(b). From Figure 6(d), the organosilanes treatment of AVF leads to a better wetting of the fibers in PHBHHx matrix. In addition, the fracture surface morphology shows a reduction in number and size of filler aggregates indicating an improved morphology. According to the literature [26], TMOS

grafted on AVF surface exhibits a bifunctional structure: the silane groups react with the hydrophilic AVF via the hydroxyl groups, while the organic part interacts with the hydrophobic polymer matrix during melt compounding.

The fracture surface morphology of PHBHHx/AVF treated with alkaline/organo-silanes combination is shown in Figure 6(e). It can be clearly observed that the surface morphology of the biocomposite is regular and homogeneous with less surface defects. Despite the presence of a very few fiber pullouts in comparison with the other biocomposite samples, this indicates improved morphology through increased interfacial adhesion between treated AVF and PHBHHx.

3.2.2. Thermal characteristics

In order to investigate the effect of various surface treatments of AVF on the thermal characteristics of PHBHHx biocomposites, DSC measurements were carried out. In this regard, thermal properties including glass transition temperature (T_g), cold crystallization temperature (T_{cc}), melting temperature (T_m), melting enthalpy (ΔH_m) and cold crystallization enthalpy (ΔH_{cc}) of PHBHHx and PHBHHx/AVF biocomposites before and after surface treatment of the fibers are provided in Table 2. From Table 2, the values of T_m , T_{cc} and T_g of PHBHHx are about 136, 63 and 2°C , respectively, which are consistent with those reported in literature [34]. It can be noticed that T_g slightly increases up on adding both untreated and treated AVF to PHBHHx, in particular for alkaline-organosilanes treated biocomposite. This is due to stiffening effect resulting from the restriction of polymer chains mobility in the amorphous phase [35]. Similar trend is also observed for T_m and T_{cc} when AVF are incorporated in PHBHHx matrix. However, the results in Table 2 show that whatever the fiber treatment of AVF, it induces almost no change on T_m and T_{cc} of PHBHHx biocomposite in comparison with the untreated one. A further trend that can be observed from the data in Table 2 is a decrease in the melting and cold crystallization enthalpies for all biocomposite

samples compared to neat PHBHHx. This is due obviously to the decrease in the reduction of PHBHHx matrix content [36–38].

Table 2

From the whole DSC data, it can be concluded that the different fiber treatment methods don't show any noticeable change in the amount of crystallinity of the biocomposite samples compared to neat PHBHHx.

3.2.3. Thermogravimetric analysis

Thermal stability of PHBHHx/AVF biocomposites subjected to various surface fiber treatments was investigated by TGA in comparison with those of untreated fibers and neat PHBHHx. TGA thermograms of the samples are shown in Figure 7. Furthermore, Table 3 summarizes the main results as the degradation temperature T_{10} corresponding to 10 wt. % mass loss, the mid-point of degradation (T_{50}) recorded at 50 wt. % mass loss, the temperature corresponding to the maximum degradation rate (T_{mdr}) and the residue at 600°C.

Figure 7

TGA thermograms show that neat PHBHHx undergoes one single decomposition step and almost no residue is observed at 600 °C. The degradation step occurs fast, and starts from almost 290°C. It is complete at approximately 310°C. The incorporation of AVF in PHBHHx results in a slight decrease in thermal stability of the biocomposite samples. Indeed, it can be noticed that T_{10} , T_{50} and T_{mdr} shift to lower temperatures, being however more pronounced for the biocomposite filled with alkaline treated fibers. The decrease in thermal stability of the biocomposites may be attributed to the moisture contained in the materials [39]; this obviously has a significant impact on the ongoing processes of polymer chain-structure degradation. Moreover, both biocomposites treated with organo-silanes and those treated with combined alkaline/organo-silanes are more stable than those filled with untreated AVF. This result indicates the effectiveness of surface fiber treatment resulting in better fiber-matrix

interactions. On the other hand, PHBHHx biocomposite filled with alkaline treated fibers shows a lower thermal stability than the untreated one, which can be explained by the slight alteration of the structure of the cellulose chains after alkaline treatment [40]. Figure 7 shows also that the TGA thermograms of the biocomposite samples exhibit clearly three decomposition steps. In the first step, located in the temperature range (160-290°C), there is a decomposition of hemicellulose [41]. The second step ranged from approximately 290-310°C, is attributed to the simultaneous decomposition of cellulose and PHBHHx. In the last step between 310 and 380°C, there is still the decomposition of both cellulose and lignin.

The characteristic temperatures are summarized in Table 3. The maximum degradation rate (T_{mdr}) of PHBHHx/AVF treated by organo-silanes and combined alkaline-organosilanes occur approximately at 293 and 292°C, respectively, which are close to that of neat PHBHHx. Untreated PHBHHx/AVF and the alkaline treated one show lower T_{mdr} comparatively to the polymer matrix. This result is logic since it is related to the simultaneous degradation of PHBHHx, cellulose and lignin [35]. In PHBHHx/alkaline treated AVF, lignin is partially or totally removed from the fibers, while in untreated AVF, the presence of impurities like pectin, waxes and other extractible, could be responsible for the decrease in T_{mdr} .

Table 3

3.2.4. Water absorption

Water absorption is mainly due to the hydrogen bonding of water molecules to the hydroxyl groups on the cellulosic fibers [42]. In this respect, Figure 8 shows the water absorption curves plotted as a function of immersion time at room temperature for neat PHBHHx and various PHBHHx/AVF biocomposites. From Figure 8, it can be observed that all curves display similar trend characterized by 2 steps. First, a fast increase in water absorption is observed in the first 24h of immersion for all samples, followed by quasi-plateau in the second step, indicating water saturation. Apparently, this looks like a Fickian behavior [43].

Furthermore, the highest water absorption is observed for alkaline treated AVF biocomposite. This behavior results from alkaline treatment, which causes a rough surface topography on AVF as observed in Figure 2(b). Moreover, alkaline treatment also leads to fiber fibrillation, which increases the effective surface area of the fiber available for absorbing water molecules [44]. The lowest water absorption is obviously for neat PHBHHx, due to its hydrophobic character. Between these 2 extreme behaviors, there are the untreated biocomposites and those treated with organosilanes and combined alkaline-organosilanes, which display water absorption rates quite close. However, the PHBHHx/AVF treated with combined alkaline-organosilanes biocomposite exhibits the lower water absorption rate. This resistance to water absorption of the organosilanes treated biocomposites may result from hydrolysable alkoxy groups of silanes which form silanols. The latter reacts with the hydroxyl groups of the fibers under moisture conditions. Stable covalent bonds at the cell wall are formed during the reaction and silanols are chemically adsorbed onto the fiber surface. Thus, the hydrocarbon chains available by applying the silanes will prevent the fiber swelling [45].

Figure 8

3.2.5. Rheological measurements

Melt rheology was used to qualitatively evaluate the filler-matrix interactions in the biocomposite [9]. In this respect, Figure 9, 10 and 11 shows respectively the curves of complex viscosity (η^*), storage modulus (G') and loss modulus (G'') versus frequency for neat PHBHHx and PHBHHx/AVF biocomposites before and after fiber surface treatments. From Figure 9, it is clearly noticed that the incorporation of both untreated and treated AVF into PHBHHx affects significantly the complex viscosity of the biocomposite at low frequencies.

Figure 9

Indeed, there is a considerable increase in η^* of the biocomposite samples compared to neat PHBHHx, being however, more pronounced for the combined alkaline-organosilanes treated

biocomposite. The incorporation of both untreated and treated AVF into PHBHHx matrix causes disturbances in the polymer flow by hindering the mobility of chains, and subsequently the increase in viscosity. Significant increases in both G' and G'' are also observed at low frequencies for all biocomposite samples as shown in Figure 10 and 11, respectively. The increase in the rheological properties of the biocomposite materials mainly at low frequencies can be attributed to occurrence of strong interactions between AVF and PHBHHx. Indeed, the storage modulus (G') and loss modulus (G'') of PHBHHx presented in Figure 10 and 11, respectively, increase considerably on adding untreated and treated AVF at 0.01 Hz, however much more pronounced for the combined alkaline-organosilanes treated AVF biocomposite. The increase is attributed to solid-like behavior as a result of strong filler-matrix interactions in agreement with the morphological data. With increasing angular frequency to almost 0.15 Hz; a pseudo-plateau is clearly noticeable in all biocomposite samples. According to Kaci et al. [45], this is attributed to strong interfacial bonding occurring between the natural fibers and the polymer matrix.

Figure 10

Figure 11

4. Conclusion

In the presented work, biocomposites based on PHBHHx and Aloe Vera fibers (AVF) have been prepared by melt compounding. The effect of various surface fiber treatments on the morphology and properties of PHBHHx biocomposites were investigated including alkaline treatment, organo-silanes treatment and combined alkaline-organosilanes treatment. From the study, it can be concluded that the surface treatment of AVF is essential to eliminate the formation of aggregates in the PHBHHx matrix and to ensure a better interfacial adhesion between the natural fibers and the polymer. Indeed, the important modification achieved with

alkaline treatment was the disruption of the hydrogen bonding in the network structure of the fibers, increasing the surface roughness and compatibility with the hydrophobic polymer. Whereas, the silane treatment of the fibers was used to promote adhesion with the PHBHHx matrix through reactions between alkoxy silanes and OH groups of AVF. The treated biocomposites exhibited increased thermal stability and rheological properties compared to untreated one, however more pronounced for PHBHHx/AVF biocomposite treated with combined alkaline-organosilanes. Furthermore, this treated biocomposite possessed the lower water absorption percentage. The results from this paper are very useful in choosing the surface treatment of fibres. Accordingly, further improvement in fiber-matrix interface has been achieved by the combined alkaline-organosilanes treatment of AVF as material reinforcement in PHBHHx biocomposites, which represent a new class of biobased and biodegradable materials. Considering their performances and the reduction of PHBHHx costs, it can be concluded that the production of such biocomposites can be an efficient and promising route to extend the PHA applications according to their great industrial potential in structural applications.

Acknowledgements

The authors are grateful to Campus France through the Tassili PHC program n°19MDU204 for its financial support in this collaborative project.

The authors are also pleased to express their grateful acknowledgements to Dr. Mickael Castro, Antoine Kervoelen, Anthony Magueresse and Françoise Peresse for their help in the experimental work.

References

- [1] C.A. Murphy, M.N. Collins, Microcrystalline Cellulose Reinforced Polylactic Acid Biocomposite Filaments for 3D Printing, *Polym. Compos.* 39 (2016) 1–10. doi:10.1002/pc.
- [2] X. Xian, X. Wang, Y. Zhu, Y. Guo, Y. Tian, Effects of MCC Content on the Structure and Performance of PLA/MCC Biocomposites, *J. Polym. Environ.* 26 (2018) 3484–3492. doi:10.1007/s10924-018-1226-3.
- [3] F. Vilaplana, E. Strömberg, S. Karlsson, Environmental and resource aspects of sustainable biocomposites, *Polym. Degrad. Stab.* 95 (2010) 2147–2161. doi:10.1016/j.polymdegradstab.2010.07.016.
- [4] S. Kennouche, N. Le, M. Kaci, J. Quantin, A. Caro-bretelle, C. Delaite, et al., Morphological characterization and thermal properties of (PHBV)/ poly (butylene succinate) (PBS)/ halloysite ternary nanocomposites, *Eur. Polym. J.* 75 (2016) 142–162. doi:10.1016/j.eurpolymj.2015.12.009.
- [5] P. Lemechko, M. Le Fellic, S. Bruzaud, Production of poly(3-hydroxybutyrate-co-3-hydroxyvalerate) using agro-industrial effluents with tunable proportion of 3-hydroxyvalerate monomer units, *Int. J. Biol. Macromol.* 128 (2019) 429–434. doi:10.1016/j.ijbiomac.2019.01.170.
- [6] T. Thomas, A. Elain, A. Bazire, S. Bruzaud, Complete genome sequence of the halophilic PHA-producing bacterium *Halomonas* sp. SF2003: insights into its biotechnological potential, *World J. Microbiol. Biotechnol.* 35(50) (2019) 1–14. doi:10.1007/s11274-019-2627-8.
- [7] L.M. Oliveira, E.S. Araújo, S.M.L. Guedes, Gamma irradiation effects on poly(hydroxybutyrate), *Polym. Degrad. Stab.* 91 (2006) 2157–2162. doi:10.1016/j.polymdegradstab.2006.01.008.
- [8] F. Valentini, A. Dorigato, D. Rigotti, A. Pegoretti, Polyhydroxyalkanoates/Fibrillated Nanocellulose Composites for Additive Manufacturing, *J. Polym. Environ.* 27 (2019) 1333–1341.
- [9] I. Zembouai, M. Kaci, L. Zaidi, S. Bruzaud, Combined effects of Sepiolite and Cloisite 30B on morphology and properties of poly(3-hydroxybutyrate-co-3-hydroxyvalerate)/polylactide blends, *Polym. Degrad. Stab.* 153 (2018) 47–52. doi:10.1016/j.polymdegradstab.2018.04.017.
- [10] Z.A. Raza, S. Abid, I.M. Banat, Polyhydroxyalkanoates: Characteristics, production, recent developments and applications, *Int. Biodeterior. Biodegrad.* 126 (2018) 45–56. doi:10.1016/j.ibiod.2017.10.001.
- [11] A. Jordá-Vilaplana, A. Carbonell-Verdú, M.D. Samper, A. Pop, D. Garcia-Sanoguera, Development and characterization of a new natural fiber reinforced thermoplastic (NFRP) with *Cortaderia selloana* (Pampa grass) short fibers, *Compos. Sci. Technol.* 145 (2017) 1–9. doi:10.1016/j.compscitech.2017.03.036.

- [12] A.N. Balaji, K.J. Nagarajan, Characterization of alkali treated and untreated new cellulosic fiber from Saharan aloe vera cactus leaves, *Carbohydr. Polym.* 174 (2017) 200–208. doi:10.1016/j.carbpol.2017.06.065.
- [13] K.J. Nagarajan, A.N. Balaji, N.R. Ramanujam, Isolation and characterization of cellulose nanocrystals from Saharan aloe vera cactus fibers, *Int. J. Polym. Anal. Charact.* 0 (2018) 1–14. doi:10.1080/1023666X.2018.1478366.
- [14] S. Chaitanya, I. Singh, Ecofriendly treatment of aloe vera fibers for PLA based green composites, *Int. J. Precis. Eng. Manuf. - Green Technol.* 5 (2018) 143–150. doi:10.1007/s40684-018-0015-8.
- [15] S. Chaitanya, I. Singh, Novel Aloe Vera fiber reinforced biodegradable composites - Development and characterization, *J. Reinf. Plast. Compos.* 35 (2016) 1411–1423. doi:10.1177/0731684416652739.
- [16] M.A. Berthet, N. Gontard, H. Angellier-Coussy, Impact of fibre moisture content on the structure/mechanical properties relationships of PHBV/wheat straw fibres biocomposites, *Compos. Sci. Technol.* 117 (2015) 386–391. doi:10.1016/j.compscitech.2015.07.015.
- [17] M. Abdelmouleh, S. Boufi, M.N. Belgacem, A. Dufresne, A. Gandini, Modification of Cellulose Fibers with Functionalized Silanes : Effect of the Fiber Treatment on the Mechanical Performances of Cellulose – Thermoset Composites, *J. Appl. Polym. Sci.* 98 (2005) 974–984. doi:10.1002/app.22133.
- [18] A. Javadi, Y. Srithep, S. Pilla, J. Lee, S. Gong, L.S. Turng, Processing and characterization of solid and microcellular PHBV/coir fiber composites, *Mater. Sci. Eng. C.* 30 (2010) 749–757. doi:10.1016/j.msec.2010.03.008.
- [19] F. Rol, M.N. Belgacem, A. Gandini, J. Bras, Recent advances in surface-modified cellulose nanofibril, *Prog. Polym. Sci.* 88 (2019) 241–264. doi:10.1016/j.progpolymsci.2018.09.002.
- [20] L. Hassaini, M. Kaci, N. Touati, I. Pillin, A. Kervoelen, S. Bruzard, Valorization of olive husk flour as a filler for biocomposites based on poly(3-hydroxybutyrate-co-3-hydroxyvalerate): Effects of silane treatment, *Polym. Test.* 59 (2017) 430–440. doi:10.1016/j.polymertesting.2017.03.004.
- [21] F. Mannai, H. Elhleli, M. Ammar, R. Passas, E. Elaloui, Y. Moussaoui, Green process for fibrous networks extraction from *Opuntia* (Cactaceae): Morphological design, thermal and mechanical studies, *Ind. Crops Prod.* 126 (2018) 347–356. doi:10.1016/j.indcrop.2018.10.033.
- [22] S. Li, S. Xu, S. Liu, C. Yang, Q. Lu, Fast pyrolysis of biomass in free-fall reactor for hydrogen-rich gas, in: *Fuel Process. Technol.*, 2004: pp. 1201–1211. doi:10.1016/j.fuproc.2003.11.043.

- [23] A.K. Varma, P. Mondal, Physicochemical Characterization and Pyrolysis Kinetic Study of Sugarcane Bagasse Using Thermogravimetric Analysis, *J. Energy Resour. Technol.* 138 (2016) 1–11. doi:10.1115/1.4032729.
- [24] L. Joyyi, M.Z. Ahmad Thirmizir, M.S. Salim, L. Han, P. Murugan, K. ichi Kasuya, et al., Composite properties and biodegradation of biologically recovered P(3HB-co-3HHx) reinforced with short kenaf fibers, *Polym. Degrad. Stab.* 137 (2017) 100–108. doi:10.1016/j.polymdegradstab.2017.01.004.
- [25] P. Georgiopoulou, E. Kontou, G. Georgousis, Effect of silane treatment loading on the flexural properties of PLA/flax unidirectional composites, *Compos. Commun.* 10 (2018) 6–10.
- [26] A. Orue, A. Jauregi, U. Unsuain, J. Labidi, A. Eceiza, A. Arbelaiz, The effect of alkaline and silane treatments on mechanical properties and breakage of sisal fibers and poly(lactic acid)/sisal fiber composites, *Compos. Part A Appl. Sci. Manuf.* 84 (2016) 186–195. doi:10.1016/j.compositesa.2016.01.021.
- [27] C.S. Wu, Assessing biodegradability and mechanical, thermal, and morphological properties of an acrylic acid-modified poly(3-hydroxybutyric acid)/wood flours biocomposite, *J. Appl. Polym. Sci.* 102 (2006) 3565–3574. doi:10.1002/app.24817.
- [28] P. Garside, P. Wyeth, Identification of cellulosic fibres by FTIR spectroscopy: Differentiation of flax and hemp by polarized ATR FTIR, *Stud. Conserv.* 51 (2006) 205–211. doi:10.1179/sic.2006.51.3.205.
- [29] C.H. Chiang, H. Ishida, J.L. Koenig, The structure of γ -aminopropyltriethoxysilane on glass surfaces, *J. Colloid Interface Sci.* 74 (1980) 396–404. doi:10.1016/0021-9797(80)90209-X.
- [30] F. Zhou, G. Cheng, B. Jiang, Effect of silane treatment on microstructure of sisal fibers, *Appl. Surf. Sci.* 292 (2014) 806–812. doi:10.1016/j.apsusc.2013.12.054.
- [31] N.P.G. Suardana, Y. Piao, J.K. Lim, Mechanical properties of hemp fibers and hemp / pp composites : effects of chemical surface treatment, *Mater. Phys. Mech.* 11 (2011) 1–8. <https://doi.org/10.1016/j.proeng.2017.07.065>.
- [32] M. Kathirselvam, A. Kumaravel, V.P. Arthanarieswaran, S.S. Saravanakumar, Characterization of cellulose fibers in *Thespesia populnea* barks: Influence of alkali treatment, *Carbohydr. Polym.* 217 (2019) 178–189. doi:10.1016/j.carbpol.2019.04.063.
- [33] M.N.K. Chowdhury, M.D.H. Beg, M.R. Khan, M.F. Mina, Modification of oil palm empty fruit bunch fibers by nanoparticle impregnation and alkali treatment, *Cellulose.* 20 (2013) 1477–1490. doi:10.1007/s10570-013-9921-7.
- [34] K.P. Shadangi, K. Mohanty, Kinetic study and thermal analysis of the pyrolysis of non-edible oilseed powders by thermogravimetric and differential scanning calorimetric analysis, *Renew. Energy.* 63 (2014) 337–344. doi:10.1016/j.renene.2013.09.039.

- [35] A. Hamma, M. Kaci, Z.A. Mohd Ishak, R. Ceccato, A. Pegoretti, Starch-grafted-polypropylene/kenaf fibres composites. Part 2: Thermal stability and dynamic-mechanical response, *J. Reinf. Plast. Compos.* 34 (2015) 2045–2058. doi:10.1177/0731684415609792.
- [36] Y. Furushima, C. Schick, A. Toda, Crystallization, recrystallization, and melting of polymer crystals on heating and cooling examined with fast scanning calorimetry, *Polym. Cryst.* 1(2018) e10005. doi:10.1002/pcr2.10005.
- [37] S.-H. Lee, S. Wang, Y. Teramoto, Isothermal Crystallization Behavior of Hybrid Biocomposite Consisting of Regenerated Cellulose Fiber, Clay, and Poly(lactic acid), *J. Appl. Polym. Sci.* 108 (2008) 870–875. doi:10.1002/app.
- [38] R.A. Shanks, A. Hodzic, S. Wong, Thermoplastic biopolyester natural fiber composites, *J. Appl. Polym. Sci.* 91 (2004) 2114–2121. doi:10.1002/app.13289.
- [39] L.J. Vandi, C.M. Chan, A. Werker, D. Richardson, B. Laycock, S. Pratt, Extrusion of wood fibre reinforced poly(hydroxybutyrate-co-hydroxyvalerate) (PHBV) biocomposites: Statistical analysis of the effect of processing conditions on mechanical performance, *Polym. Degrad. Stab.* 159 (2019) 1–14. doi:10.1016/j.polymdegradstab.2018.10.015.
- [40] Z. Yang, H. Peng, W. Wang, T. Liu, Comparison of the Thermal Degradation of Natural, Alkali-Treated and Silane-Treated Hemp Fibers Under Air and an Inert Atmosphere, *J. Appl. Polym. Sci.* 112 (2009) 226–234. doi:10.1002/app.
- [41] A. Aboulkas, K. El Harfi, A. El Bouadili, Non-isothermal kinetic studies on co-processing of olive residue and polypropylene, *Energy Convers. Manag.* 49 (2008) 3666–3671. doi:10.1016/j.enconman.2008.06.029.
- [42] M. Kaci, H. Djidjelli, A. Boukerrou, L. Zaidi, Effect of wood filler treatment and EBAGMA compatibilizer on morphology and mechanical properties of low density polyethylene/olive husk flour composites, *Express Polym. Lett.* 1 (2007) 467–473. doi:10.3144/expresspolymlett.2007.65.
- [43] M. Haghghi-Yazdi, J.K.Y. Tang, P. Lee-Sullivan, Moisture uptake of a polycarbonate blend exposed to hygrothermal aging, *Polym. Degrad. Stab.* 96 (2011) 1858–1865. doi:10.1016/j.polymdegradstab.2011.07.007.
- [44] M.H. Hamidon, M.T.H. Sultan, A.H. Ariffin, A.U.M. Shah, Effects of fibre treatment on mechanical properties of kenaf fibre reinforced composites: A review, *J. Mater. Res. Technol.* 8 (2019) 3327–3337. doi:10.1016/j.jmrt.2019.04.012.
- [45] M. Kaci, A. Hamma, I. Pillin, Y. Grohens, Effect of reprocessing cycles on the morphology and properties of poly(propylene)/wood flour composites compatibilized with ebagma terpolymer, *Macromol. Mater. Eng.* 294 (2009) 532–540. doi:10.1002/mame.200900089.

Caption of figures

Scheme 1. Chemical structure of PHBHHx.

Figure 1. Leaves of Aloe Vera Cactus.

Figure 2. Extraction steps of Aloe Vera fibers by water-immersion process.

Figure 3. ATR-IR spectra of untreated Aloe Vera fibers and those treated with alkaline, organosilane and alkaline-organosilane combination.

Figure 4. SEM micrographs of surface morphology of AVF. (a): before fiber surface treatment and (b): after alkaline treatment.

Figure 5. DTG curves of untreated and alkali, silane and combined alkali-silane treated AVF.

Figure 6. SEM micrographs of neat PHBHHx: (a), PHBHHx/UAVF: (b), PHBHHx/ATAVF: (c), PHBHHx/STAVF: (d) and PHBHHx/A-STAVF: (e).

Figure 7. TGA thermograms of PHBHHx and PHBHHx/AVF biocomposites before and after various surface fiber treatments.

Figure 8. Water uptake curves versus time recorded at room temperature for PHBHHx and PHBHHx/AVF biocomposites before and after surface fiber treatments.

Figure 9. Complex viscosity (η^*) curves versus frequency for neat PHBHHx and PHBHHx/AVF biocomposites.

Figure 10. Curves of storage modulus (G') versus frequency for neat PHBHHx and PHBHHx/AVF biocomposites.

Figure 11. Curves of loss modulus (G'') versus frequency for neat PHBHHx and PHBHHx/AVF biocomposites.

Caption of tables

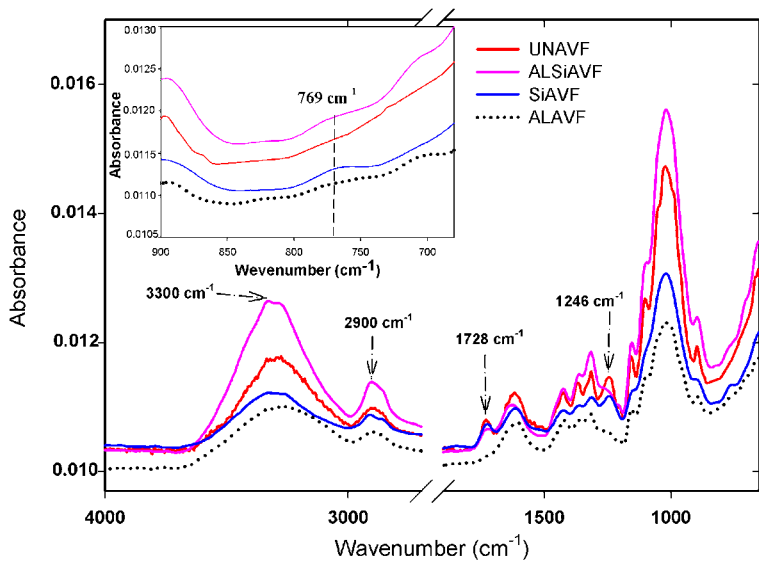
Table 1. Code and composition of neat PHBHHx and biocomposite formulations based on PHBHHx/AVF.

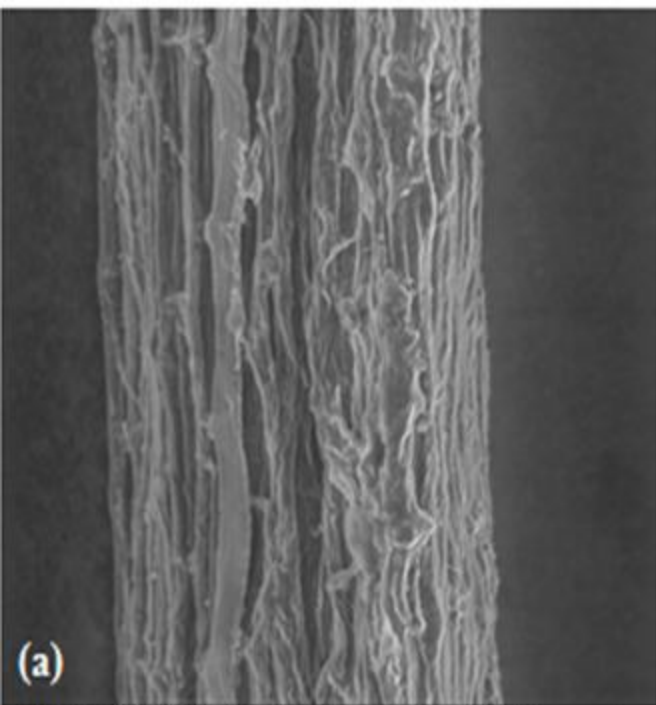
Table 2. Values of T_g , T_{cc} , T_m , ΔH_{cc} and ΔH_m of neat PHBHHx and PHBHHx/AVF biocomposites before and after various fiber surface treatments.

Table 3. Values of T_{10} , T_{50} , T_{mdr} and % residue of neat PHBHHx and PHBHHx biocomposites before and after surface fiber treatments.





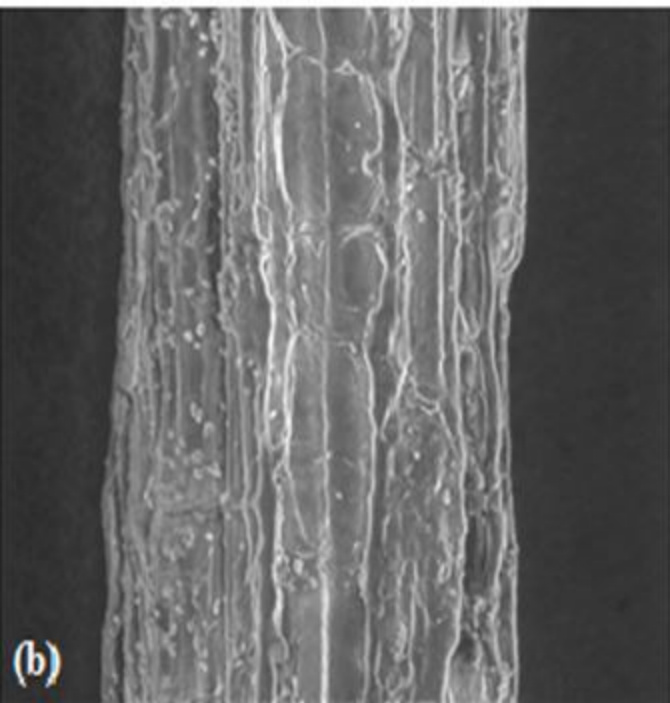




(a)

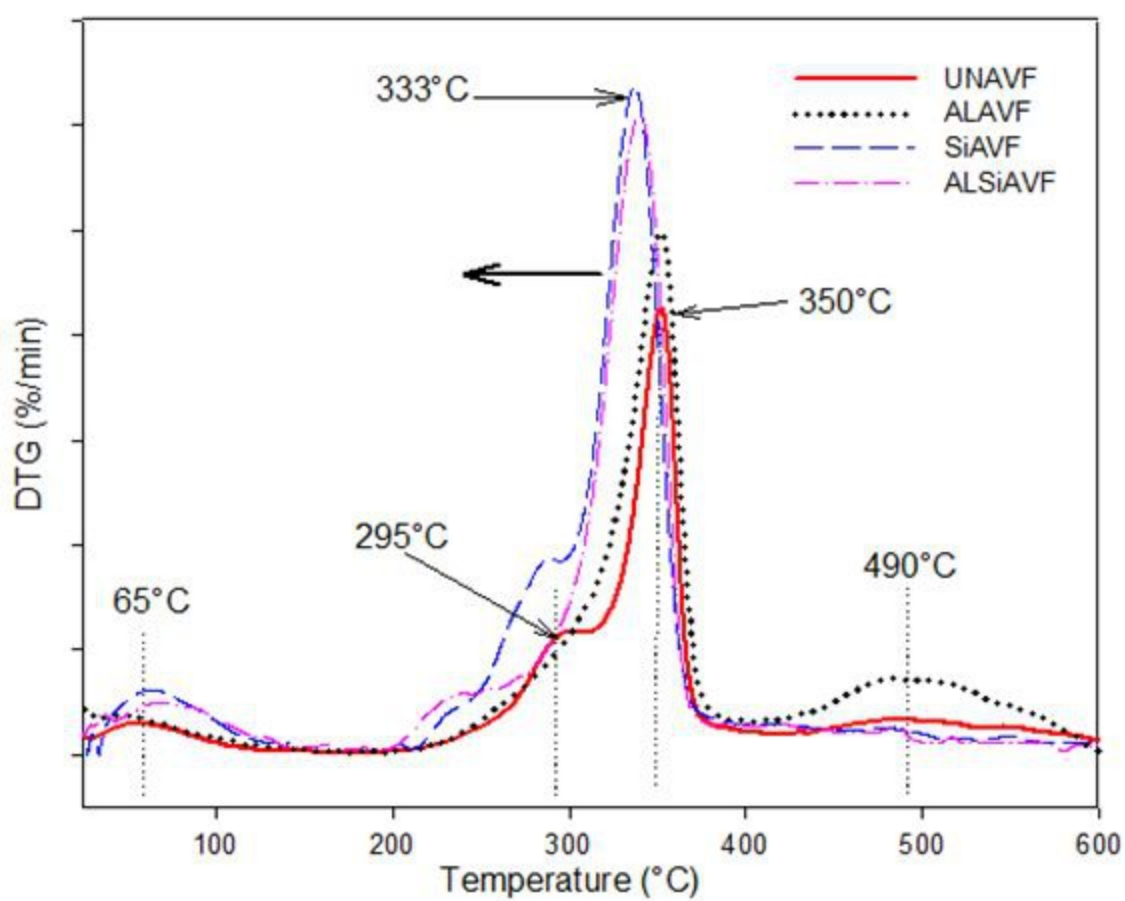
HV WD Spot Sig Det Mag Pressure
12.5 kV 9.4 mm 4.0 SE LFD 1000x 0.75 Torr

100.0 μm



HV WD Spot Sig Det Mag Pressure
12.5 kV 9.3 mm 4.0 SE LFD 1000x 0.75 Torr

100 μ m

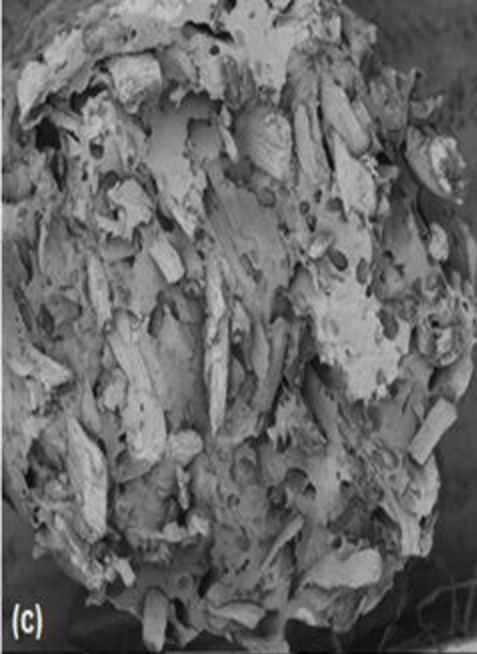





(a)

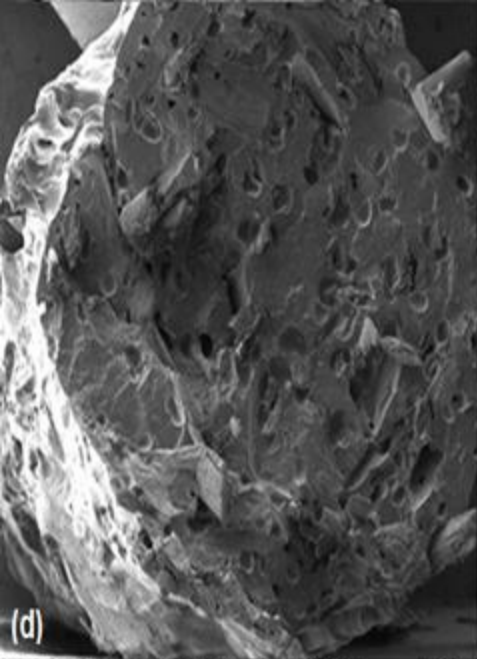




(b)

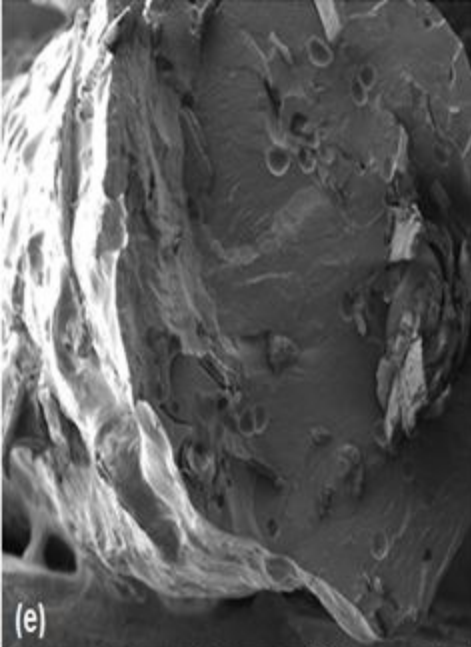


(c)

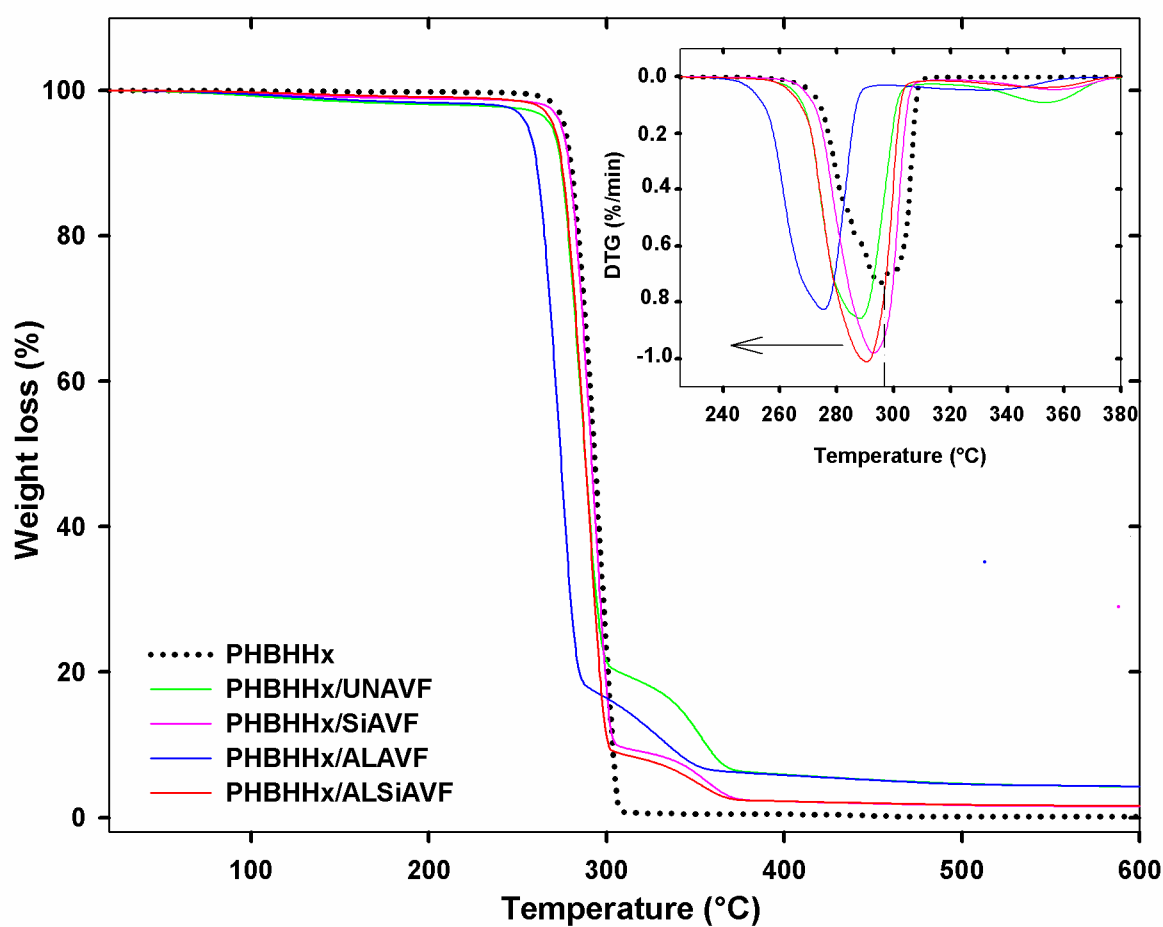
BED-C 3.0 kV WD 12.6 mm Std.-PC 75.0 HighVac.  x35  500 μ m

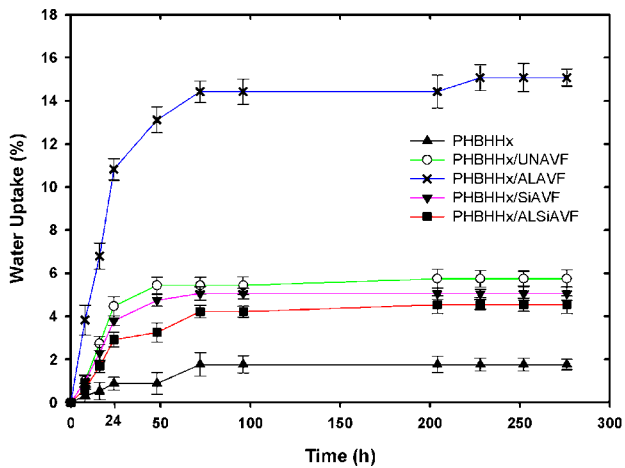


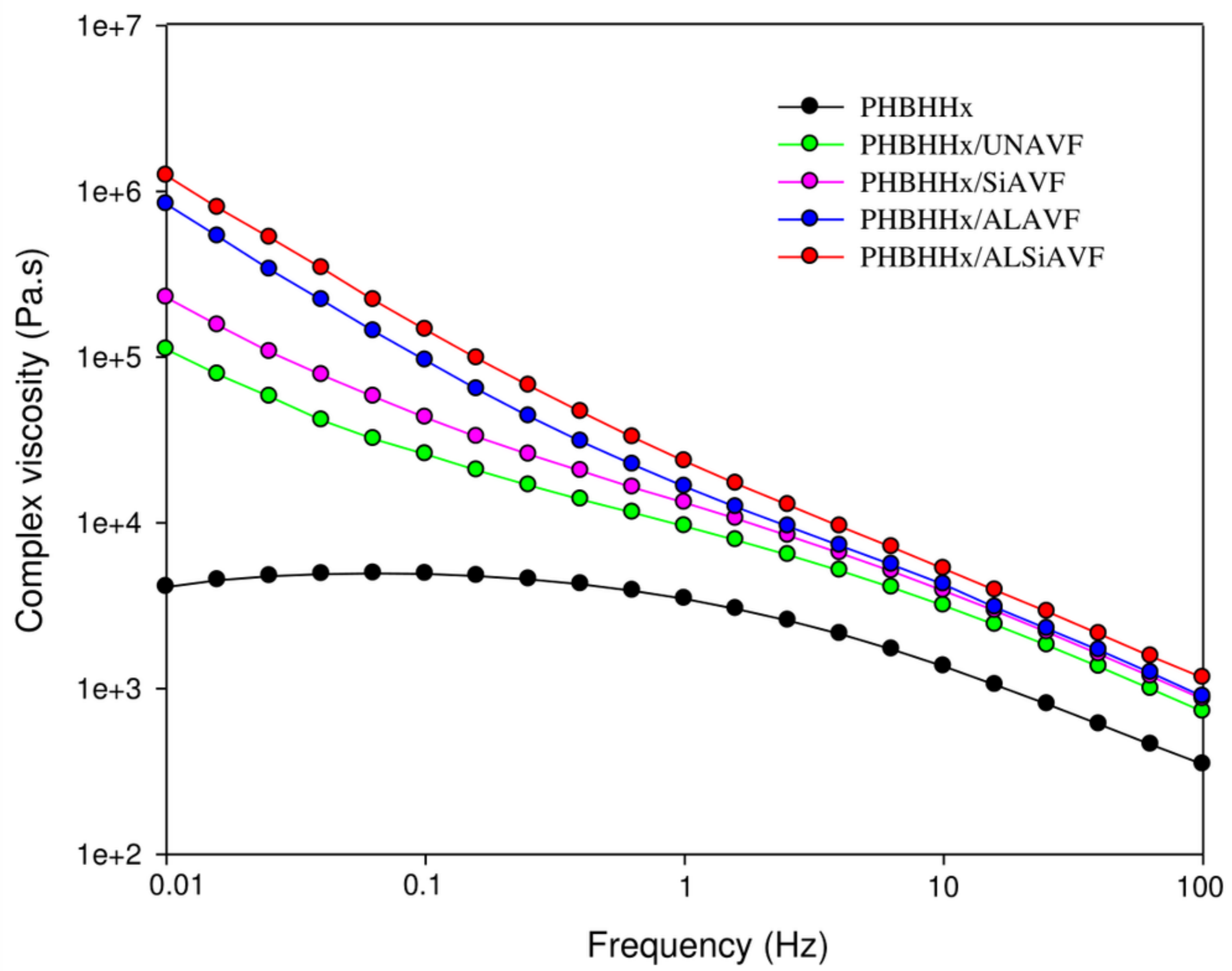
(d) BED-C 3.0 kV WD 12.6 mm Std.-PC 75.0 HighVac.  x35  500 μ m

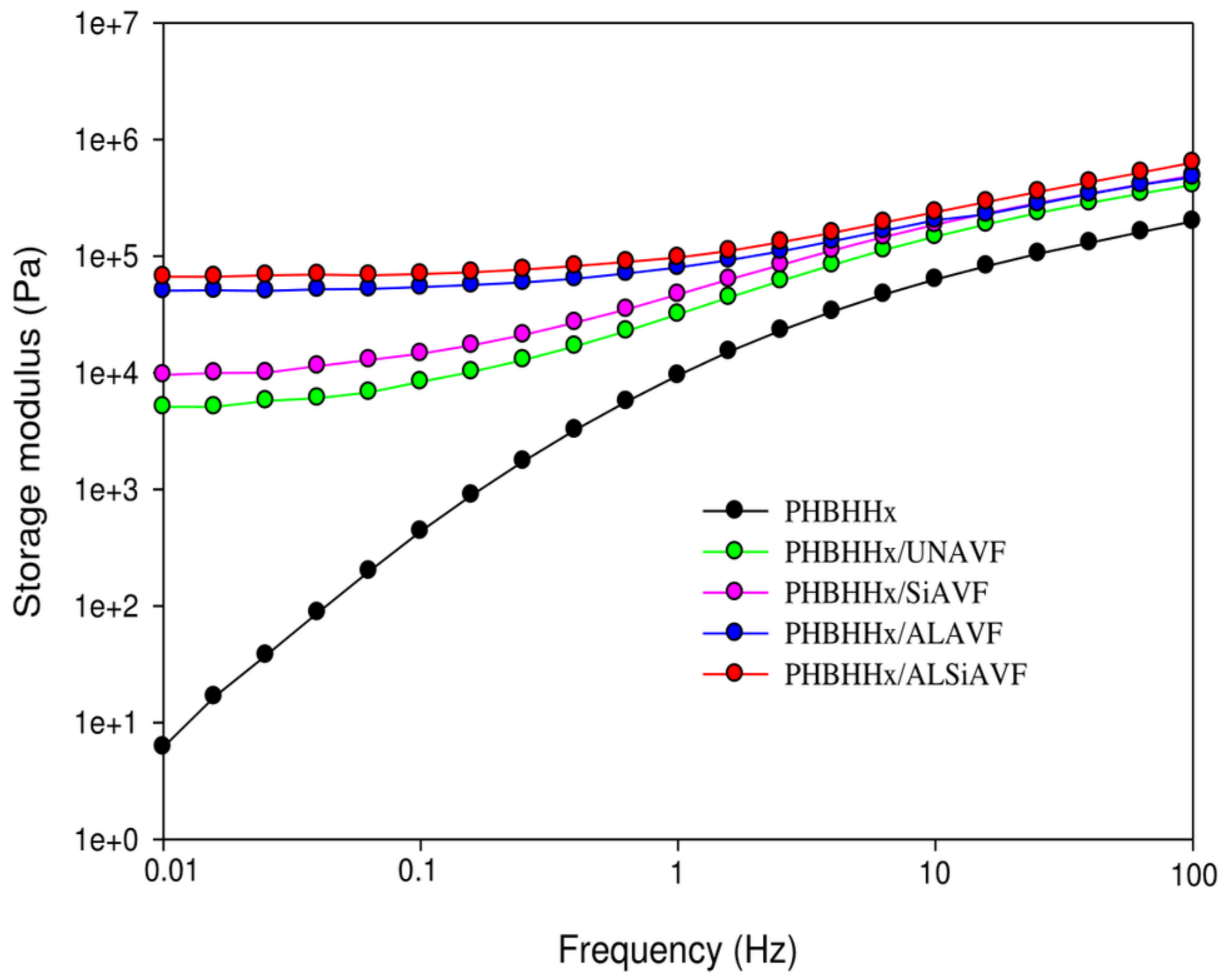


(e)









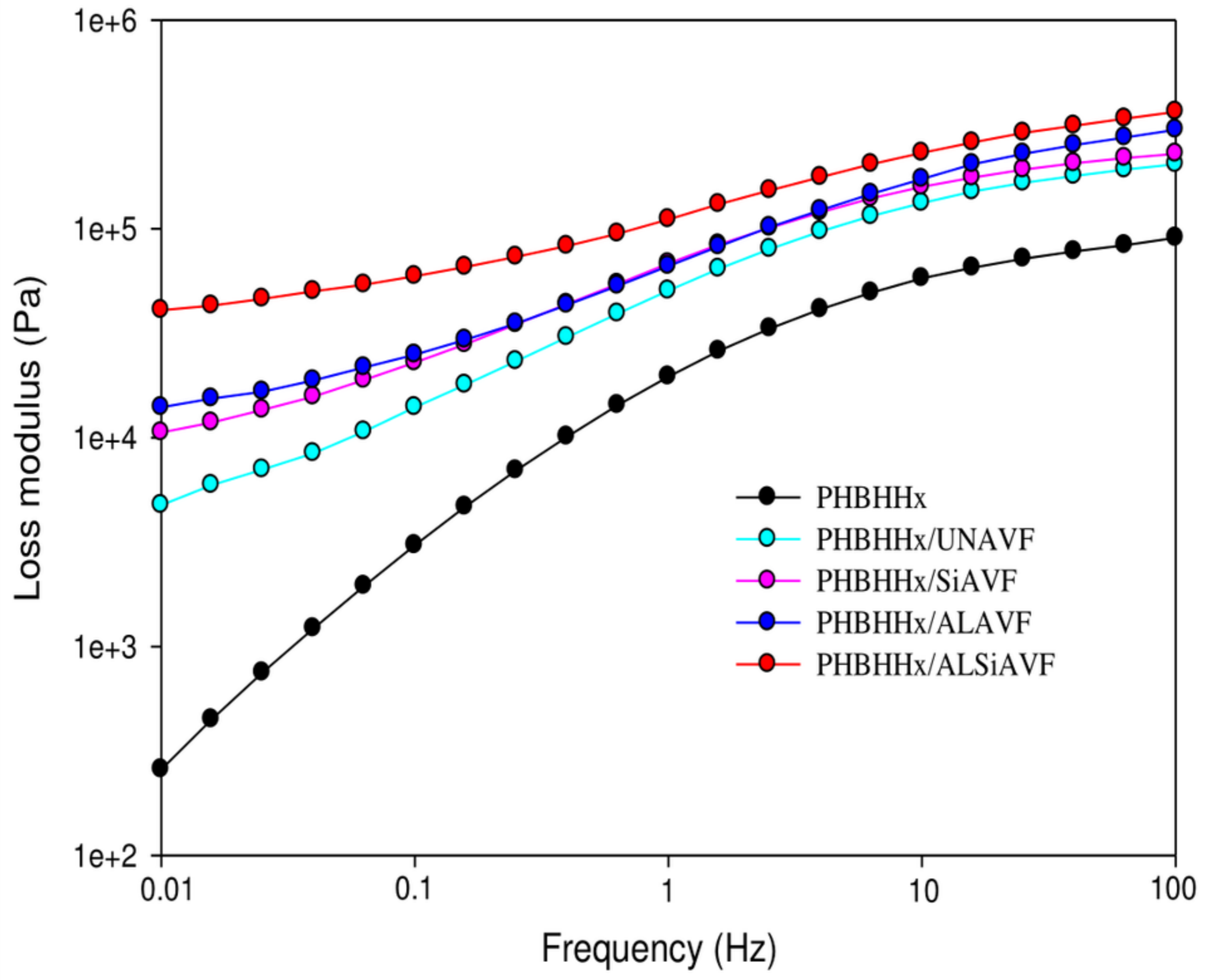


Table 1. Code and composition of neat PHBHHx and PHBHHx/AVF biocomposites formulations.

Sample codes	PHBHHx (wt.%)	AVF (wt.%)	Designation
PHBHHx	100	-	Matrix
PHBHHx/UNAVF	80	20	PHBHHx/Untreated AVF
PHBHHx/ALAVF	80	20	PHBHHx/alkaline treated AVF
PHBHHx/SiAVF	80	20	PHBHHx/organosilanes treated AVF
PHBHHx/ALSiAVF	80	20	PHBHHx/combined alkaline and organosilanes treated AVF

Table 2. Values of T_g , T_{cc} , T_m , ΔH_{cc} and ΔH_m of neat PHBHHx and PHBHHx/AVF biocomposites before and after various fiber surface treatments.

Samples	T_g (°C)	T_{cc} (°C)	T_m (°C)	ΔH_{cc} (J/g)	ΔH_m (J/g)
PHBHHx	2.2±0.1	63.1±1.1	136.1±0.9	37.2±0.2	25.2±0.5
PHBHHx/UNAVF	2.3±0.7	65.2±3.9	137.2±2.5	34.1±1.7	21.9±1.6
PHBHHx/ALAVF	2.9±0.8	66.7±1.9	136.4±2.3	27.8±2.1	17.9±2.5
PHBHHx/SiAVF	2.7±0.4	65.4±2.2	136.5±1.8	36.7±1.6	22.7±0.7
PHBHHx/ALSiAVF	3.6±0.3	65.3±2.0	138.3±0.5	31.6±1.2	21.8±0.9

Table 3. Values of T_{10} , T_{50} , T_{mdr} and % residue of neat PHBHHx and PHBHHx biocomposites before and after surface fiber treatments.

Samples	T_{10} (°C)	T_{50} (°C)	T_{mdr} (°C)	Char yield (%)
PHBHHx	280±0.5	294±1.8	295±1.1	0.2±0.05
PHBHHx/UNAVF	274±0.8	288±1.9	288±0.8	4.2±0.6
PHBHHx/ALAVF	260±0.7	274±1.7	276±0.9	4.3±0.4
PHBHHx/SiAVF	278±0.4	293±1.3	293±0.3	1.9±0.1
PHBHHx/ALSiAVF	277±0.2	289±1.1	292±0.3	1.6±0.1